arXiv:1508.03197v1 [cond-mat.str-el] 13 Aug 2015

Thermodynamic properties of the 2D frustrated Heisenberg model for the entire $J_1 - J_2$ circle

A.V. Mikheyenkov[1,2,3] [*], A.V. Shvartsberg[2], V.E. Valiulin[2] and A.F. Barabanov[1]
[1] Institute for High Pressure Physics RAS, 142190 Moscow (Troitsk), Russia
[2] Moscow Institute of Physics and Technology, 141700 Dolgoprudny, Russia
[3] National Research Centre 'Kurchatov Institute', 123182 Moscow, Russia

August 14, 2015

Abstract

Using the spherically symmetric self-consistent Green's function method, we consider thermodynamic properties of the $S = 1/2$ J_1-J_2 Heisenberg model on the 2D square lattice. We calculate the temperature dependence of the spin-spin correlation functions $c_{\mathbf{r}} = \langle S^z_{\mathbf{0}} S^z_{\mathbf{r}} \rangle$, the gaps in the spin excitation spectrum, the energy E and the heat capacity C_V for the whole J_1–J_2-circle, i.e. for arbitrary φ, $J_1 = cos(\varphi)$, $J_2 = sin(\varphi)$. Due to low dimension there is no long-range order at $T \neq 0$, but the short-range holds the memory of the parent zero-temperature ordered phase (antiferromagnetic, stripe or ferromagnetic). $E(\varphi)$ and $C_V(\varphi)$ demonstrate extrema "above" the long-range ordered phases and in the regions of rapid short-range rearranging. Tracts of $c_{\mathbf{r}}(\varphi)$ lines have several nodes leading to nonmonotonic $c_{\mathbf{r}}(T)$ dependence. For any fixed φ the heat capacity $C_V(T)$ always has maximum, tending to zero at $T \to 0$, in the narrow vicinity of $\varphi = 155^\circ$ it exhibits an additional frustration-induced low-temperature maximum. We have also found the nonmonotonic behaviour of the spin gaps at $\varphi = 270^\circ \pm 0$ and exponentially small antiferromagnetic gap up to ($T \lesssim 0.5$) for $\varphi \gtrsim 270^\circ$.

PACS codes
75.10.Jm Quantized spin models, including quantum spin frustration
75.10.Kt Quantum spin liquids, valence bond phases and related phenomena
75.30.Kz Magnetic phase boundaries

Contents

1 Introduction 2

2 Spherically symmetric self-consistent approach 4

3 The ground state properties 6

4 Thermodynamic properties 7

---

[*] mikheen@bk.ru

5 Discussion and summary **9**
5.1 AFM order . . . 9
5.2 Spin liquid . . . 10
5.3 Stripe order . . . 10
5.4 FM order . . . 11
5.5 Specific heat . . . 11
5.6 Fine tuning of the method . . . 13
5.7 Summary . . . 13

1 Introduction

Investigation of low-dimensional quantum magnets have attracted much attention during the last years (see [1] for a review). Frustrated two-dimensional (2D) and quasi-2D magnets are of particular interest, as they demonstrate strong quantum fluctuations effects. The 2D spin-1/2 J_1–J_2 quantum Heisenberg model is a conventional tool for the investigation of frustration effects and quantum phase transitions (see, e.g., [2–7]).

Cuprates and numerous other quasi-2D compound with antiferromagnetic (AFM) nearest-neighbour (NN) and next-nearest neighbour (NNN) couplings $J_1 > 0, J_2 > 0$ have been investigated experimentally for years [8–11]

This class of systems has been recently expanded by several magnetic materials with a ferromagnetic (FM) NN coupling $J_1 < 0$ and a frustrating AFM NNN coupling $J_2 > 0$, e.g., $Pb_2VO(PO_4)_2$ [12–15], $(CuCl)LaNb_2O_7$ [16], $SrZnVO(PO_4)_2$ [15, 17, 18], and $BaCdVO(PO_4)_2$ [14, 17, 19]. The frustrating J_2 is believed to be large enough to drive these materials out of the FM phase. There are also materials, such as K_2CuF_4, Cs_2CuF_4, Cs_2AgF_4, La_2BaCuO_5, and Rb_2CrCl_4, [20–23] with insufficiently strong frustrating AFM NNN interaction.

The general picture can be seen from Figure 1, where the phase diagram of 2D J_1–J_2 model in the classical limit $S \to \infty$ is complemented by the positions of several experimental systems. Hereinafter the J_1–J_2-circle is defined by $J_1 = cos(\varphi)$, $J_2 = sin(\varphi)$. In the classical limit only three phases are realized — all with long-range order (LRO) — AFM, FM and stripe (in the quantum case $S = 1/2$ disordered phases appear between stripe and FM, as well as between stripe and AFM).

The Hamiltonian of the model has the form

$$H = J_1 \sum_{\langle \mathbf{i},\mathbf{j} \rangle} \widehat{\mathbf{S}}_\mathbf{i} \widehat{\mathbf{S}}_\mathbf{j} + J_2 \sum_{[\mathbf{i},\mathbf{j}]} \widehat{\mathbf{S}}_\mathbf{i} \widehat{\mathbf{S}}_\mathbf{j} \tag{1}$$

where $(\widehat{\mathbf{S}}_\mathbf{i})^2 = 3/4$, $\langle \mathbf{i}, \mathbf{j} \rangle$ denotes NN bonds and $[\mathbf{i}, \mathbf{j}]$ denotes NNN bonds of the square lattice sites $\mathbf{i}, \mathbf{j}$.

The theoretical investigation of the model in the first quadrant $J_1 > 0, J_2 > 0$ was detonated by the HTSC breakthrough and led to innumerable number of papers (see, e.g. [24, 25] and references therein). In a nutshell, the generally accepted result is the following. At $T = 0$ the system undergoes two successive phase transitions: from AFM LRO to disordered phase and then to stripe LRO (see, for example, recent calculations [26] and references therein). The nature of these quantum phase transitions and the detailed structure of the disordered state remains debatable.

The unfrustrated FM case ($J_1 < 0, J_2 = 0$) has been also widely investigated, e.g., by the modified spin-wave theory [27, 28], renormalization group approaches [29, 30], the quantum Monte Carlo method [31–34] and by a spherically symmetric self-consistent approach (SSSA) — spin-rotation-invariant Green's function method (RGM) in alternative notation — [35–39].

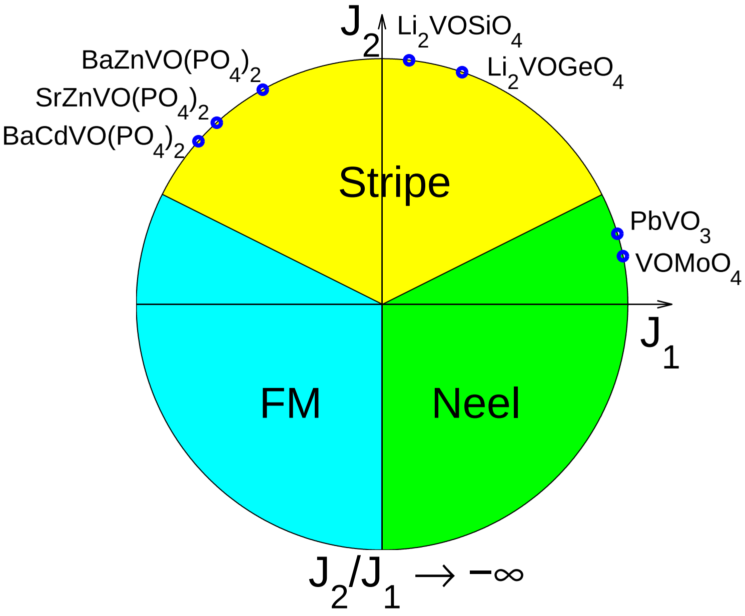

Figure 1: (Color online) Circle phase diagram of the 2D J1-J2 Heisenberg model in classical limit; points on the circle correspond to exchange parameters of several layered compounds, data from [19]

Recent experiments with vanadates and related compounds have stimulated theoretical studies of the J_1–J_2 model with $J_1 < 0$ and frustrating $J_2 > 0$. [40–51]. It was found that in the second quadrant there is also a disordered ground state between FM and stripe. Rough estimates for the transition points in both quadrants are $J_2 \sim \pm 0.4 J_1$ (AFM → disordered, FM → disordered) and $J_2 \sim \pm 0.7 J_1$ (disordered → stripe). Note that for the classical model ($S \to \infty$) there are only two transitions at points $J_2 = \pm 0.5 J_1$ (AFM → stripe, FM → stripe).

So, one has several experimental points settled on the upper half of the J_1–J_2-circle and a set of theoretical methods, each being tuned for a particular parameter region. A unified approach, which can describe the entire picture, both for the ground state and the thermodynamics of the model, is obviously desirable. It is also interesting to look at the lower half of the circle ($J_2 < 0$), though still experimentally unobtainable.

The SSSA proved to be the appropriate approach. SSSA preserves the spin SU(2) and translation symmetries of the Hamiltonian and allows:

i. to satisfy automatically the Marshall and MerminWagner theorems

ii. to describe at $T = 0$ (when the LRO is possible) the system states both with and without LRO in the frames of one and the same approach

iii. to find the microscopic characteristics such as the spin-excitation spectrum $\omega(\mathbf{q})$, the spin-gaps T-dependence and the explicit form of the dynamic susceptibility $\chi(\mathbf{q}, \omega, T)$; to go beyond the mean-field approximation by introducing damping in the expression for the spin Greens function $G(\mathbf{q}, \omega)$ [7].

Note, that for the 1D spin-1/2 Heisenberg ferromagnet it was shown that the RGM reproduces Bethe-ansatz results [37, 52].

Let us also mention that SSSA has been applied to another lattice geometry, $S > 1/2$ [53], the systems with the anisotropic spin exchange — iron pnictides AFe_2As_2 (A = Ca, Sr, Ba) — [54] and to 2D J_1–J_2–J_3 model [7, 55, 56].

We have recently considered the ground state of the model (1) $J_1{-}J_2$ circle [57]. In particular, it was shown that at $T=0$ the transitions between all ordered and disordered phases are continuous, except the transition FM→AFM at $J_1=0,\ J_2=-1$.

In the present work we turn to the nonzero temperatures and consider thermodynamic properties. We calculate the temperature dependence of the spin-spin correlation functions, the gaps in the spin excitation spectrum and the heat capacity. As in [57], the model is treated in SSSA.

The paper is organized as follows: in Sec. 2 and Sec. 3 we briefly remind the spherically symmetric self-consistent approach for two-time retarded Green's functions and the results of [57] for $T=0$. In Sec. 4 we present the results for the thermodynamic properties. Discussion and summary are given in Sec. 5.

2 Spherically symmetric self-consistent approach

As already mentioned, the calculations are performed in SSSA for the spin-spin Green's function [7,35,36,48,49,58,59].

$$G_{\mathbf{nm}}=\langle S^z_{\mathbf{n}}|S^z_{\mathbf{m}}\rangle_{\omega+i\delta}=-i\int\limits_0^\infty dt\, e^{i\omega t}\langle[S^z_{\mathbf{n}}(t),S^z_{\mathbf{m}}]\rangle \tag{2}$$

Due to the spherical symmetry, only the Green's functions diagonal with respect to $\alpha=x,y,z$ are nonzero, mean cite spin is zero ($G^{zz}=G^{xx}=G^{yy}$; $\langle S^\beta_{\mathbf{n}}\rangle=0$, $\beta=x,y,z$). There are three branches of spin excitations degenerate with respect to β. Because $\langle[S^z_{\mathbf{n}},S^z_{\mathbf{m}}]\rangle=0$ and $[S^\alpha_{\mathbf{n}};S^\beta_{\mathbf{m}}]=i\delta_{\mathbf{nm}}\varepsilon_{\alpha\beta\gamma}S^\gamma_{\mathbf{n}}$, we have for $G_{\mathbf{nm}}$

$$\omega G_{\mathbf{nm}}=\langle[S^z_{\mathbf{n}},S^z_{\mathbf{m}}]\rangle+\langle[S^z_{\mathbf{n}},\hat{H}]|S^z_{\mathbf{m}}\rangle_{\omega+i\delta}=i\sum_{\mathbf{b=g,d}}J_{\mathbf{b}}\langle(S^x_{\mathbf{n+b}}S^y_{\mathbf{n}}-S^y_{\mathbf{n+b}}S^x_{\mathbf{n}})|S^z_{\mathbf{m}}\rangle_{\omega+i\delta} \tag{3}$$

where $J_g=J_1,\ J_d=J_2$. The second differentiation step leads to three-site Green's functions:

$$\begin{gathered}
i\omega\sum_{\mathbf{b=g,d}}J_{\mathbf{b}}\langle(S^x_{\mathbf{n+b}}S^y_{\mathbf{n}}-S^y_{\mathbf{n+b}}S^x_{\mathbf{n}})|S^z_{\mathbf{m}}\rangle_{\omega+i\delta}=2\sum_{\mathbf{b=g,d}}J_{\mathbf{b}}C_{\mathbf{b}}(\delta_{\mathbf{n+b,m}}-\delta_{\mathbf{n,m}})-\\
-\frac{1}{2}\sum_{\mathbf{b=g,d}}J^2_{\mathbf{b}}(G_{\mathbf{n+b,m}}-G_{\mathbf{nm}})-\sum_{\mathbf{b,b'};\beta\neq z;\,\mathbf{b+b'}\neq 0}J_{\mathbf{b}}J_{\mathbf{b'}}[\langle S^\beta_{\mathbf{n+b}}S^z_{\mathbf{n-b'}}S^\beta_{\mathbf{n}}|S^z_{\mathbf{m}}\rangle_{\omega+i\delta}-\\
-\langle S^\beta_{\mathbf{n+b}}S^\beta_{\mathbf{n-b'}}S^z_{\mathbf{n}}|S^z_{\mathbf{m}}\rangle_{\omega+i\delta}+\langle S^z_{\mathbf{n+b}}S^\beta_{\mathbf{n+b+b'}}S^\beta_{\mathbf{n}}|S^z_{\mathbf{m}}\rangle_{\omega+i\delta}-\langle S^\beta_{\mathbf{n+b}}S^z_{\mathbf{n+b+b'}}S^\beta_{\mathbf{n}}|S^z_{\mathbf{m}}\rangle_{\omega+i\delta}]\}
\end{gathered} \tag{4}$$

where $c_{\mathbf{b}}=\langle S^z_{\mathbf{n+b}}S^z_{\mathbf{n}}\rangle$.

In the mean-field approximation, the subsequent procedure amounts to decoupling the chain of the equations of motion at the second step using the triple-site term splitting of the characteristic form

$$\begin{gathered}
S^j_{\mathbf{n+g_1+g_2}}S^l_{\mathbf{n+g_1}}S^\gamma_{\mathbf{n}}\approx\alpha_{\mathbf{g}}(\delta_{jl}\left\langle S^j_{\mathbf{n+g_1+g_2}}S^l_{\mathbf{n+g_1}}\right\rangle S^\gamma_{\mathbf{n}}+\\
+\delta_{l\gamma}\left\langle S^l_{\mathbf{n+g_1}}S^\gamma_{\mathbf{n}}\right\rangle S^j_{\mathbf{n+g_1+g_2}})+\alpha_{\mathbf{g_1+g_2}}\delta_{j\gamma}\left\langle S^j_{\mathbf{n+g_1+g_2}}S^\gamma_{\mathbf{n}}\right\rangle S^l_{\mathbf{n+g_1}}
\end{gathered} \tag{5}$$

where $\alpha_{\mathbf{g}}$ and $\alpha_{\mathbf{g_1+g_2}}$ are vertex corrections. In the general case vertex corrections can depend on cite indices, hereafter we use the simplest one-vertex approximation [35,36,48,57], i.e. all the vertices are taken to be equal. We emphasize that in the case of $S=1/2$ the splitting procedure for each term is unambiguous because in (4) $\beta\neq z$, and the average involves two spins with $\beta\neq z$.

After the Fourier transformation

$$S^z_{\mathbf{q}} = \frac{1}{\sqrt{N}} \sum_{\mathbf{r}} e^{-i\mathbf{qr}} S^z_{\mathbf{r}} \tag{6}$$

solution of equations (3) and (4) leads to the Green's function $G(\mathbf{q},\omega) = \langle S^z_{\mathbf{q}} | S^z_{-\mathbf{q}} \rangle_\omega = -\chi(\mathbf{q},\omega)$

$$G(\mathbf{q},\omega) = \frac{F_{\mathbf{q}}}{(\omega^2 - \omega^2_{\mathbf{q}})} \tag{7}$$

In the case of $J_1 - -J_2$ model the expressions for $F_{\mathbf{q}}$ and $\omega^2_{\mathbf{q}}$ are the following:

$$F_{\mathbf{q}} = -8 \left[J_1 c_g (1-\gamma_g) + J_2 c_d (1-\gamma_d) \right]; \tag{8}$$

$$\omega^2_{\mathbf{q}} = 2[(\gamma_1 K_1 + \gamma_2 K_2) - (\gamma_3 K_3 + \gamma_4 K_4) - (\gamma_5 K_5 + \gamma_6 K_6)] \tag{9}$$

The variables $K_1 ... K_6$ involved in the expression for the spectrum are given by

$$K_1 = J_1 J_2 K_{gd} + 12 J_1^2 \widetilde{c}_g + 1 + K_{gg}; \quad K_2 = J_1 J_2 K_{gd} + 12 J_2^2 \widetilde{c}_d + 1 + K_{dd} \tag{10}$$

$$K_3 = 16 J_1^2 \widetilde{c}_g; \quad K_4 = 16 J_2^2 \widetilde{c}_d; \quad K_5 = 16 J_1 J_2 \widetilde{c}_g; \quad K_6 = 16 J_1 J_2 \widetilde{c}_d \tag{11}$$

$$K_{gg} = \sum_{\substack{\mathbf{r}=\mathbf{g}_1+\mathbf{g}_2; \\ \mathbf{g}_1 \neq -\mathbf{g}_2}} \widetilde{c}_r; \; K_{dd} = \sum_{\substack{\mathbf{r}=\mathbf{d}_1+\mathbf{d}_2; \\ \mathbf{d}_1 \neq -\mathbf{d}_2}} \widetilde{c}_r; \; K_{gd} = \sum_{\mathbf{r}=\mathbf{g}+\mathbf{d}} \widetilde{c}_r \tag{12}$$

$$\begin{aligned} \gamma_1 &= 1-\gamma_g; \; \gamma_2 = 1-\gamma_d; \; \gamma_3 = 1-\gamma_g^2; \; \gamma_4 = 1-\gamma_d^2; \; \gamma_5 = (1-\gamma_g)\gamma_d; && (13) \\ \gamma_6 &= (1-\gamma_d)\gamma_g; \quad \gamma_g = \frac{1}{2}(\cos q_x + \cos q_y); \quad \gamma_d = \cos q_x \cos q_y && (14) \end{aligned}$$

where $\widetilde{c}_r$ stands for the correlators, renormalized by the vertex correction $\widetilde{c}_r = \alpha c_r$ (in (9) we rearranged the contributions to the spectrum in a different manner, than in [48, 49]).

The Green's function $G(\mathbf{q},\omega)$ involves the correlators $c_{\mathbf{r}}$ for the first five coordination spheres $\mathbf{r} = \mathbf{g}, \mathbf{d}, 2\mathbf{g}, \mathbf{g}+\mathbf{d}, 2\mathbf{d}$, which must be evaluated self-consistently in terms of $G(\mathbf{q},\omega)$. In addition, $G(\mathbf{q},\omega)$ must satisfy the spin constraint $c_{\mathbf{r}=\mathbf{0}} = \langle S^z_{\mathbf{i}} S^z_{\mathbf{i}} \rangle = 1/4$ (sum rule). These conditions are

$$c_{\mathbf{r}} = \frac{1}{N} \sum_{\mathbf{q}} c_{\mathbf{q}} e^{i\mathbf{qr}}; \; c_{\mathbf{q}} = \left\langle S^z_{\mathbf{q}} S^z_{-\mathbf{q}} \right\rangle = -\frac{1}{\pi} \int_0^\infty d\omega \; (2m(\omega)+1) \, \mathrm{Im} G^{zz}(\omega,\mathbf{q}); \tag{15}$$

$$c_{\mathbf{r}=\mathbf{0}} = 1/4 \; = -\frac{1}{\pi} \frac{1}{N} \sum_{\mathbf{q}} \int_0^\infty d\omega \; (2m(\omega)+1) \, \mathrm{Im} G^{zz}(\omega,\mathbf{q}); \tag{16}$$

The system of self-consistent equations is then solved numerically. Hereafter all the energy-related parameters are set in the units of $J = \sqrt{J_1^2 + J_2^2}$.

In the general case, in the framework of (3), (4), both short-range order (SRO) and long-range order (LRO) states can be realized. Because the dimension is equal to two, only SRO are possible at $T \neq 0$, and both possibilities can take place as $T \to 0$ (LRO is characterized by nonzero spin–spin correlators at infinity $\langle S^\alpha_{\mathbf{r}} S^\alpha_{\mathbf{0}} \rangle_{r\to\infty}$).

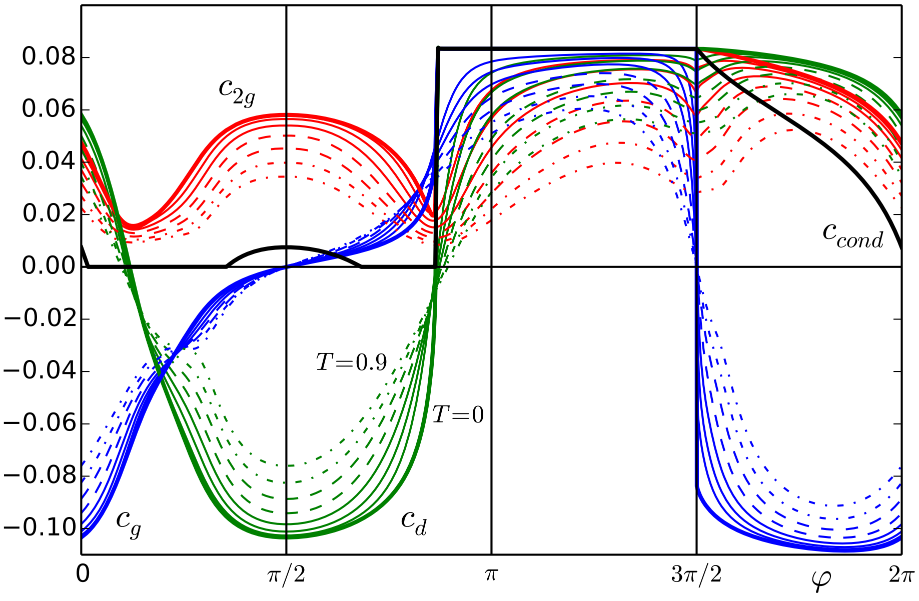

Figure 2: (Color online) Condensate c_{cond} (black bold line) and correlation functions on the first three coordination spheres as functions of the angle parameter φ ($J_1 = \cos\varphi$, $J_2 = \sin\varphi$) — c_g (blue), c_d (green) and c_{2g} (red); bold lines correspond to the zero temperature, solid lines — to $T = 0.3, 0.4, 0.5$, dashed lines — to $T = 0.6, 0.7$ and dotted lines — to $T = 0.8, 0.9$.

3 The ground state properties

For $T \neq 0$ the system is always in the SRO state (the spin-liquid state). For small T, the function $c_{\mathbf{q}}$ is always peaked near the point $\mathbf{q}_0$ where the spin gap is minimum (except for the zero point $\mathbf{q} = 0$, where spin gap is always zero, but $c_{\mathbf{q}}$ is not peaked because $F_{\mathbf{q}=\mathbf{0}} = 0$).

Two cases are possible as $T \to 0$. In the first case, the system remains in the SRO state, the gap is not closed, and the contribution of $m(\omega)$ to $c_{\mathbf{q}}$ in (15) vanishes as $T \to 0$.

In the second case, as the temperature decreases, the system passes into the LRO state, and the gap goes to zero at a point $\mathbf{q}_0$, which for $J_1 - J_2$ model can be either $\mathbf{q}_0 = \mathbf{Q} = (\pi, \pi)$, (corresponding to antiferomagnetic LRO) or $\mathbf{q}_0 = \mathbf{X} = (\pi, 0)$; $(0, \pi)$ (stripe LRO). The zero gap leads to the existence of condensate c_{cond}, which determines spin-spin correlation function at infinity. That is nonzero condensate means the LRO existence at zero temperature.

The case of FM LRO is somewhat different. The condensate at the point $\mathbf{q}_0 = \mathbf{\Gamma} = (0, 0)$ does appear for $T \to 0$, but the spin gap at $\mathbf{q}_0$ is closed for any temperature. In this case the transition to LRO is governed by the spectrum transformation near $\mathbf{q}_0$ — from linear to quadratic (see detailes in [57]).

Note that the third exchange interaction J_3 being added to the model changes the LRO picture qualitatively — the helical LRO becomes possible. In the $J_1 - J_2 - J_3$ model the condensate peak point in the structure factor can be located not only at $\mathbf{\Gamma}$, $\mathbf{Q}$, or $\mathbf{X}$, but also at arbitrary incommensurate point on the side or diagonal of the Brillouin zone [7, 46, 55, 56, 60].

The resulting picture for the whole region of J_1 and J_2 exchanges ("J_1–J_2 circle") [57] is shown in Figures 2,4. As seen in the figures, four types of the ground state are possible: AFM, stripe, FM and the disordered spin-liquid state (two different areas — SL^1 and SL^2). Note, that in the frames of SSSA the transition SL^2 →FM appears to be continuous ([57]).

Let us remind, that in SSSA mean spin projection is always zero $\langle S^z_{\mathbf{n}}\rangle = 0$ and any possible ground state preserves the whole — translational and spin SU(2) — symmetry of the Hamiltonian. The LRO, if it does exist (this possibility is open — LRO is possible only at $T = 0$) is determined by the spin-spin correlation function at infinity.

At $\varphi = 0$ ($J_1 = 1$, $J_2 = 0$), as it the classical limit, the ground state is AFM. Quantum fluctuations destroy LRO with the increasing φ (that is increasing J_2) and the system transforms to the disordered state SL^1. Note, that different alternative states are considered to be competitive in the locality of LRO disappearance at $T = 0$. These are in particular columnar and box phases which preserve the SU(2) symmetry, but brake the translational one (see [61] for recent review). The disordered state in SSSA is always spin-liquid-like in the above noted sense and it can not be distinguished from the mentioned alternatives with nearby energies.

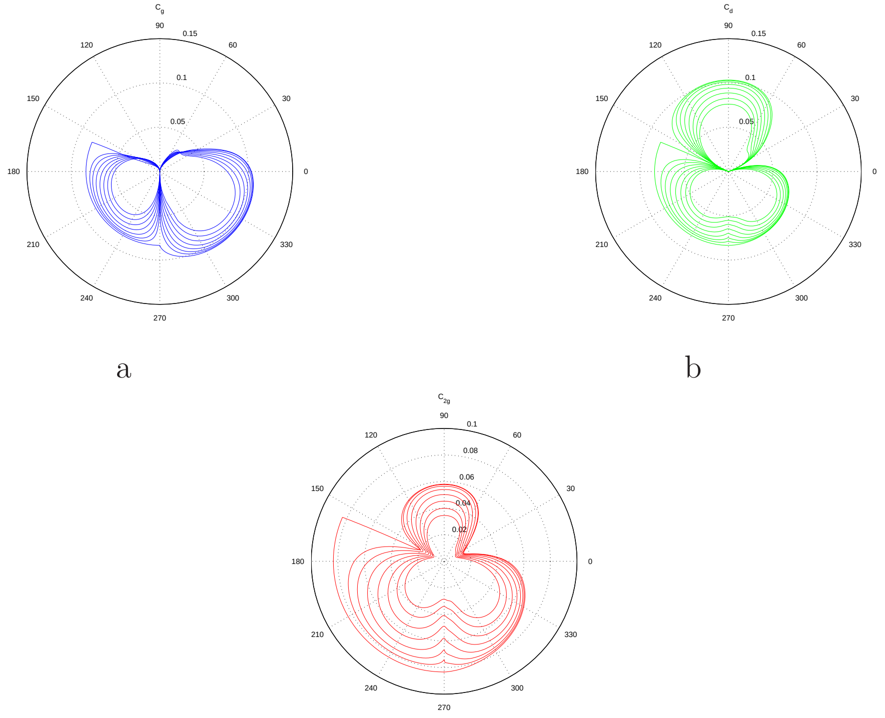

a

b

c

Figure 3: (Color online) Polar diagrams for the absolute values of the first (a), second (b) and third (c) correlation functions ($|c_g|$, $|c_d|$, and $|c_{2g}|$ correspondingly); outer lines correspond to $T = 0$, inner lines — to $T = 0.3 \div 0.9$.

In the vicinity of $\varphi = \pi/2$ there exists another ordered state, with stripe LRO type. Then with the increasing φ the spin liquid appears again (SL^2, its SRO differing from that of SL^1). After SL^2 the system continuously transforms to FM-LRO state. And the last transition — at $\varphi = 3\pi/4$ restores the AFM LRO. In the frames of SSSA all the mentioned transitions at $T = 0$ are continuous, except the last one.

4 Thermodynamic properties

The results of our calculations for the spin-spin correlation finctions on the first, second and third coordination spheres ($c_{\mathbf{g}}$, $c_{\mathbf{d}}$ and $c_{2\mathbf{g}}$ correspondingly) at different temperatures ($0 \leq T \leq 0.8$) are presented in Figure 2.

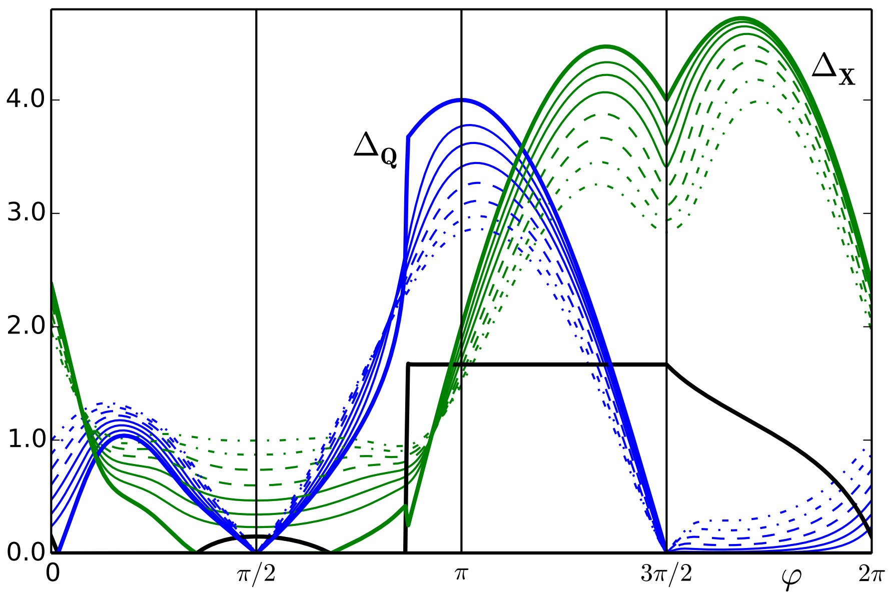

Figure 4: (Color online) Spin gaps $\Delta_{\mathbf{Q}}$ (blue) and $\Delta_{\mathbf{X}}$ (green) at points $\mathbf{Q} = (\pi, \pi)$ and $\mathbf{X} = (\pi, 0), (0, \pi)$ as functions of the angle parameter φ ($J_1 = \cos\varphi$, $J_2 = \sin\varphi$); bold lines correspond to the zero temperature, solid lines — to $T = 0.3, 0.4, 0.5$, dashed lines — to $T = 0.6, 0.7$ and dotted lines — to $T = 0.8, 0.9$. Black bold line corresponds to the value of condensate function c_{cond} (in altered scale).

As it is seen from the figure, at nonzero temperatures the SRO of the disordered state holds the memory of the parent zero-temperature ordered phase. The region overlying the AFM phase is characterized by AFM-like correlators $c_g < 0$, $|c_g| > c_d > c_{2g} > 0$, the region above stripe phase – by stripe-like ones $c_d < 0$, $c_{2g} > 0$, $|c_d| > c_{2g} > |c_g|$, and the area above FM phase – by FM-like $c_g > c_d > c_{2g} > 0$. In the intermediate regions SRO transforms from one limit to another.

It is natural to expect simultaneous decrease of all the correlators absolute values with the temperature growth. In the main so it is. There are, however, two important exceptions with inverse temperature dependence. It is firstly the nearest correlator c_g in the region of small J_1 – above the stripe phase, in part of SL^1 and in the whole SL^2 region; secondly, NN correlator c_d in narrow vicinities of the nodes – in the middle of SL^1 and near the transition SL^2 →FM (see Sec. 5 for the explanations).

The general view of the correlators temperature behaviour can be also seen in Figure 3a, Figure 3b and Figure 3c, where polar diagrams for the correlators absolute values are shown. These figures allow to compare the SRO structure with the initial classical phase diagram. In particular, it is clearly seen, that in the region corresponding to classical stripe phase the nearest correlator $|c_g|$ is an order of magnitude smaller than the next-nearest one $|c_d|$. The regions of c_g and c_d inverse temperature dependence can be also seen.

The gap in the spin excitations spectrum at zero point $\mathbf{\Gamma}$ =(0, 0) of the Brillouin zone is zero $\Delta_{\mathbf{\Gamma}} = 0$ in any phase at any temperature. The temperature dependence of spin gaps $\Delta_{\mathbf{Q}}$ and $\Delta_{\mathbf{X}}$ at two another symmetrical points — AFM point $\mathbf{Q} = (\pi, \pi)$ and (equivalent) stripe points $\mathbf{X} = (0, \pi), (\pi, 0)$ — is shown in Fig. 4 (the corresponding polar diagrams – Fig. 5a Fig. 5b).

Figure 6 shows the results for heat capacity $C_V(\varphi)$ at different temperatures. Two next figures — Figures 7, 8 — show the detailed temperature dependencies for several values of φ (in the

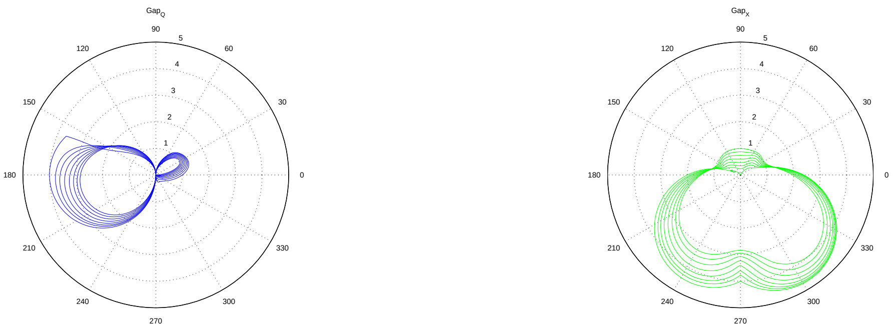

a b

Figure 5: (Color online) Polar diagrams for the spin gaps $\Delta_{\mathbf{Q}}$ (a) and $\Delta_{\mathbf{X}}$ (b) (compare with Fig.4).

temperature intervals, where the adopted computational scheme leads to satisfactory convergence). The two mentioned figures demonstrate in particular, that the temperature curve for heat capacity has a peak for any chosen value of φ.

5 Discussion and summary

Hereinafter we discuss the most interesting properties of the phase diagram obtained. Let us remind, that the LRO is absent at $T \neq 0$ and all the "circle" $0 \leq \varphi \leq 2\pi$ is covered by spin-liquid. Nevertheless we will classify the $T \neq 0$ phase diagram regions by the LRO type at $T = 0$.

5.1 AFM order

5.1.1

A dramatic difference of the $T = 0$ LRO strength (the value of spin-spin correlator at infinity) at points $\varphi = 0$ ($J_1 = 1$, $J_2 = 0$) and $\varphi = 3\pi/2 + 0$ ($J_1 = +0$, $J_2 = -1$) is worth noting.

That is the infinitesimal AFM NN exchange with the FM NNN (diagonal) exchange equal to unity leads to much more strong LRO than in the case of conventional AFM with NN AFM exchange equal to unity. The SRO difference between these two points (both at zero and nonzero temperatures) is not so large.

5.1.2

In the interval between $\varphi = 3\pi/2 + 0$ and $\varphi \sim 330°$ (Figure 4 and Figure 5a) the AFM spin gap is small ($\Delta_{\mathbf{Q}} \ll T$) up to high enough temperatures ($T \lesssim 0.5$). At the conventional AFM point $\varphi = 0$ the gap becomes exponentially small at much lower temperatures ($T \lesssim 0.05 \ll 0.5$). When $\Delta_{\mathbf{Q}} \ll T$ the gap $\Delta_{\mathbf{Q}}$ determines the AFM correlation length $\xi_{AFM} \sim \Delta_{\mathbf{Q}}^{-1}$. So the correlation length increases greatly from the point $\varphi = 0$ to the interval $3\pi/2 \leq \varphi \lesssim 330°$ (that is consistent with the mentioned LRO evolution).

Note, that, as it can be shown, at $\varphi = 0$ the exponentially small gap at high temperatures $T \sim 0.5$ is realized for the spin $S \geq 1$.

5.2 Spin liquid

5.2.1

Let us note the dissimilarity of the spin liquid evolution (with growing φ) in two areas, corresponding to zero-temperature regions SL^1 and SL^2. The SL^1 liquid at $T = 0$ exists in the angle range $0.051 \le \varphi \le 1.111$ ($2.92^\circ \le \varphi \le 57.30^\circ$), it is between AFM and stripe phases. The SRO in SL^1 smoothly transforms from the left bank to the right one, from the AFM-type ($c_g < 0$, $|c_g| > c_d > c_{2g} > 0$) to the stripe-type ($c_d < 0$, $c_{2g} > 0$, $|c_d| > c_{2g} > |c_g|$). That is not the case for SL^2 liquid ($2.141 \le \varphi \le 2.712$ ($122.67^\circ \le \varphi \le 155.39^\circ$) at $T = 0$, the region between stripe and FM phases). Almost in the whole SL^2 area the SRO is stripe-like, in particular, c_d remains negative. The absolute value of c_d almost everywhere, except tiny region near $\varphi = 2.712$, is larger than the nearest neighbour correlator c_g. And only close to FM border the drastic restructuring of the correlators takes place. At $T \neq 0$, as it was repeatedly mentioned, there is no LRO, but all the above statements concerning SRO do hold.

5.2.2

As it was noted earlier, there are regions of the phase diagram with anomalous temperature behaviour of the correlators at fixed φ (absolute value growing with temperature or nonmonotonic behaviour).

This anomaly for c_g correlator realizes in the region from the middle of SL^1 phase through the stripe-phase and all the SL^2 up to the transition to FM. The anomalous regions for c_d correlator — narrow areas near the nodes — are in the middle of SL^1 and near $SL^2 \to$FM transition. The reason for c_d anomaly is obviously the following. For different temperatures $c_d(\varphi)$ changes sign at different points φ. The normal temperature behaviour of the correlator would pass to the normal one after crossing φ axis only if the node of the correlators cone should be exactly on the φ axis (that is $c_d(\varphi_0, T) = 0$ for any T). But generally there is no physical reason for this statement.

The reasons for other mentioned temperature anomaly — the $c_g(\varphi, T)$ behaviour — are not so obvious. Presumably it is connected to the rapid SRO rearrangement.

5.3 Stripe order

The most interesting point of the area is $\varphi = \pi/2$ ($J_1 = 0$, $J_2 = 1$). At this point the lattice is decoupled into two non-interacting sublattices. One can see from Figure 2, that, as it should be, at any temperature $c_d\,(\pi/2) = c_g\,(0)$, $c_{2g}\,(\pi/2) = c_d\,(0)$. The decoupling means that $c_g(\pi/2, T)$ is strictly zero. That is why the cone of c_g correlators with anomalous T-behaviour retains the anomalous behaviour after crossing the node on φ axis.

At the same point the AFM gap $\Delta_{\mathbf{Q}}(\varphi = \pi/2) = 0$ for any temperature (see Figure 4), though AFM LRO at any temperatures, including $T = 0$, is absent.

Formally it follows from the analytical expression for the AFM gap $\Delta_{\mathbf{Q}}(\varphi = \pi/2) \sim J_1$. The naive explanation is that the system is degenerate with respect to mutual rotation of the sublattices, that is the transfer of spin excitation to the neighbouring cite costs no energy.

All the same is true for the point $\varphi = 3\pi/2$ ($J_1 = 0$, $J_2 = -1$). Though is this case there is AFM LRO at $\varphi = 3\pi/2 + 0$ and $T = 0$ (and FM LRO at $\varphi = 3\pi/2 - 0$, $T = 0$).

5.4 FM order

5.4.1 $\mathrm{SL}^2 \rightarrow$ FM transition

As it was noted earlier, it was shown in [57], that $\mathrm{SL}^2 \rightarrow$ FM transition at $T = 0$ is continuous, though it takes place in the very narrow φ interval. At $T \neq 0$, as it is seen in Figures 2–5, in the vicinity of this transition the c_{2g} temperature dependence is nonmonotonic and the temperature dependencies of other correlators and the gaps are inverse. The heat capacity (as function of φ) at any temperature has sharp minimum near this transition (Figures 6–8).

5.4.2 FM $\rightarrow$ AFM transition

This transition takes place at $\varphi = 3\pi/2$. At this point the lattice is splitted into two noninteracting sublattices. At $\varphi \rightarrow 3\pi/2 - 0$ there is no frustration with respect to the FM order, at $\varphi \rightarrow 3\pi/2 + 0$ — no frustration with respect to the AFM order. Therefore it is physically obvious that in the quantum limit at $T = 0$ a transition between these two phases is of the first order and there is no spin-liquid area between FM an AFM. Our previous calculations [57] do confirm this evidence. At nonzero temperatures the transition is obviously continuous. But as it is seen from Figures 2–5, the correlator $c_g(\varphi)$ rapidly transforms and changes the sign. Other correlators and the spin gaps demonstrate nonmonotonic dependence on φ, the heat capacity has sharp minimum.

Note once more, that near $\varphi = 270 + \Delta\varphi$ the AFM gap $\Delta_{\mathbf{Q}}$ is exponentially small up to $T \sim 0.5$. $\Delta_{\mathbf{Q}} \sim 10^{-4} - 10^{-5}$ for $\Delta\varphi \sim 5^o$. That is why our calculation can not reproduce the fine structure of the correlators and the heat capacity for $\varphi = 270 + \Delta\varphi$ at low temperatures.

5.5 Specific heat

As it is seen from Figures 6–8 the heat capacity for any φ tends to zero at $T \rightarrow 0$. The reason is the stabilization of all the correlators (and the energy) at low temperatures. At any fixed φ the heat capacity T-dependence, as it should, has the maximum, varying in its height and position (see Figure 7, Figure 8).

It is also seen from Figure 6 that there always exists a local minimum of the function $C_V(\varphi)$ inside the areas above the ordered phases (AFM, stripe and FM), if T is not too high. The reason is that the correlators (and the energy) in the corresponding areas weakly depend on φ. These minima correspond to local minima of the energy $E(\varphi)$.

Three other local minima of $C_V(\varphi)$ are observed, on the contrary, in the regions of neighbouring short-range orders rivalry, where the correlators are rapidly rearranging, and the energy also weakly depends on φ. These minima correspond to local maxima of the energy $E(\varphi)$.

Five of the mentioned points of $C_V(\varphi)$ local minima are marked by diamonds in Figure 6. The heat capacity temperature dependencies $C_V(T)$ at these points and symmetrically neighbouring points are shown in Figures 7, 8.

Figure 7 corresponds to φ in the middle of ordered (at $T = 0$) Stripe and AFM phases. It is interesting that the heat capacity $C_V(\varphi, T)$ is symmetric on φ relative to the minima of $C_V(\varphi)$ and $E(\varphi)$ in a wide T range. The situation in the region above the FM phase is slightly different, because, as it is seen from Figure 6, $C_V(\varphi)$ moves with temperature.

Figure 8 corresponds to φ in the regions of the strong frustration where different short-range orders concur. The heat capacity $C_V(\varphi, T)$ is symmetric on φ relative to the minimum of $C_V(\varphi)$ and maximum $E(\varphi)$ in a wide T range. The case of $\varphi = 155^\circ \pm 5^\circ$ is obviously notable. As in other cases symmetrical satellite $C_V(T)$ lines are similar, but the central line $C_V(\varphi = 155^\circ, T)$ demonstrates additional maximum at low T. This maximum was found and discussed in [48]. The

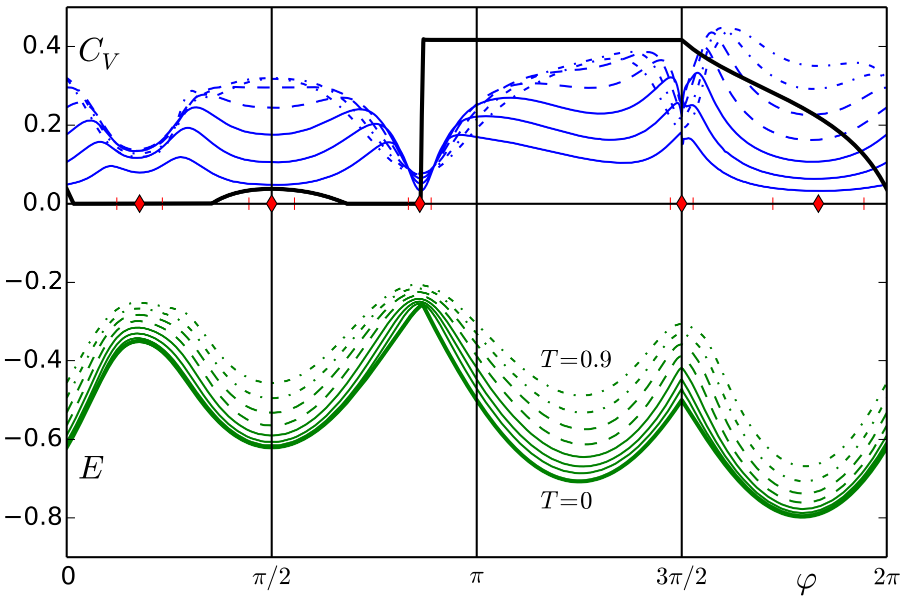

Figure 6: (Color online) Specific heat C_V (blue) and energy per site E (green) as functions of the angle parameter φ ($J_1 = \cos\varphi,\ J_2 = \sin\varphi$). Bold green line corresponds to the energy of the ground state ($T = 0$). Solid lines correspond to $T = 0.3, 0.4, 0.5$, dashed lines — to $T = 0.6, 0.7$ and dotted lines — to $T = 0.8, 0.9$. Black bold line corresponds to the value of condensate function c_{cond} (in altered scale). The $C_V(T)$ slices for φ values marked by diamonds and tics are shown in Figures 7-8.

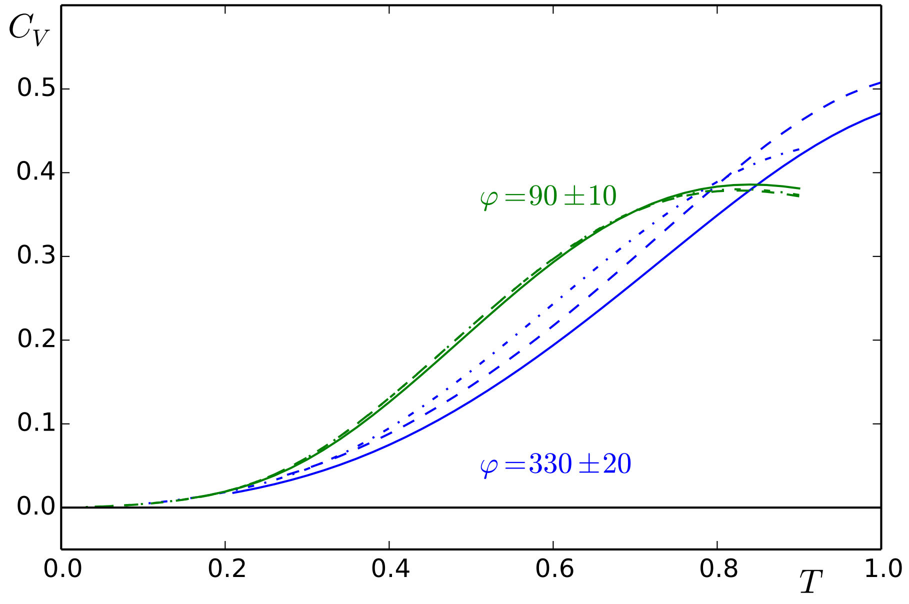

Figure 7: (Color online) Families of the specific heat $C_V(T)$ curves near values of angle parameter φ ($J_1 = \cos\varphi,\ J_2 = \sin\varphi$) corresponding to $C_V(\varphi)$ minima above FM and AFM phases (see Figure 6).

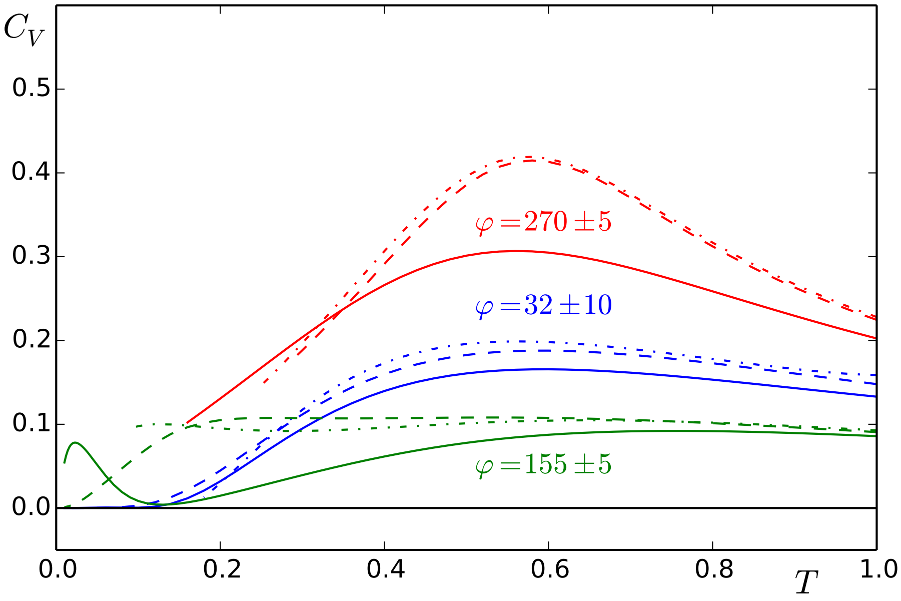

Figure 8: (Color online) Families of the specific heat $C_V(T)$ curves near values of angle parameter φ ($J_1 = \cos\varphi$, $J_2 = \sin\varphi$) corresponding to $C_V(\varphi)$ minima above the regions of SRO rearranging (see Figure 6). $C_V(T, \varphi = 155°)$ demonstrates two maxima – see text.

low-temperature frustration-induced maximum $C_V(T)$ was also found in 1D case for $S = 1/2$ and $S = 1$ [62].

5.6 Fine tuning of the method

As it was noted above, all the calculations in the present work has been carried out in the straight and simple approximation, without any tuning parameters. The tuning in SSSA is commonly made via different manipulations with vertex corrections [7, 31, 35, 36, 48, 49, 52, 54–59, 62] or accounting for complex structure of the Green's function, that is, considering the polarization operator (in particular, accounting for damping of spin excitations) [7, 55, 56].

All such complications obviously affect the results. At very low T the obtained quantitative differences can amount significant values. Figure 9 demonstrates, that even the simplest self-consistent accounting for the damping in the frames of the Green's function

$$G_\gamma^{zz}(\omega, \mathbf{q}) = \frac{F_\mathbf{q}}{\omega^2 - \omega_\mathbf{q}^2 + i\omega\gamma} \tag{17}$$

(γ — damping parameter) shifts the borders of the disordered phase between AFM and stipe phases at $T = 0$.

Nevertheless, our estimates and comparison of the available data confirm, that the reasonable degree of tuning does not lead to any topological modifications of the phase diagram.

5.7 Summary

To summarize, in the present work thermodynamic properties of of the 2D $J_1 - J_2$ $S = 1/2$ Heisenberg model are considered for the entire phase diagram the frames of one and the same approach — spherically symmetric self-consistent approach for two-time retarded Green's functions.

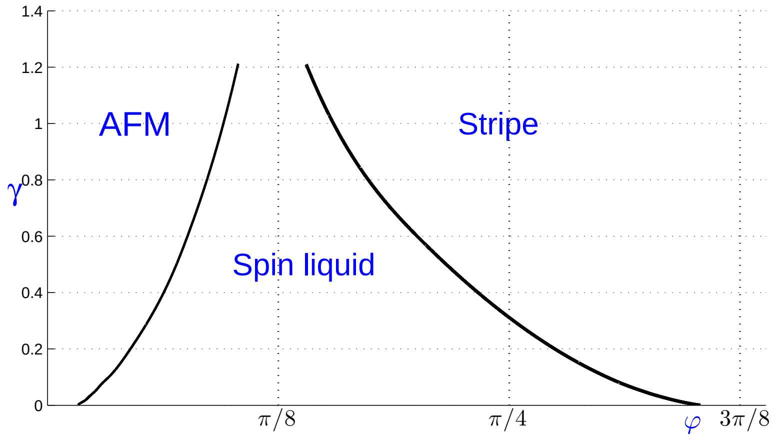

Figure 9: (Color online) Effect of the damping parameter γ on the phase boundaries of the spin liquid SL^1.

This work is supported by Russian Foundation for Basic Research, grant 13-02-00909a.

References

[1] H. T. Diep, ed., *Frustrated Spin Systems*, World Scientific, Singapore, 2-nd edn. (2013).

[2] P. Chandra and B. Doucot, Phys. Rev. B **38**, 9335 (1988).

[3] H. J. Schulz and T. A. L. Ziman, Europhys. Lett. **18**, 355 (1992).

[4] A. E. Trumper, L. O. Manuel, C. J. Gazza et al., Phys. Rev. Lett. **78**, 2216 (1997).

[5] L. Capriotti, F. Becca, A. Parola et al., Phys. Rev. Lett. **87**, 097201 (2001).

[6] R. R. P. Singh, W. Zheng, J. Oitmaa et al., Phys. Rev. Lett. **91**, 017201 (2003).

[7] A. F. Barabanov, A. V. Mikheyenkov, and A. V. Shvartsberg, Theor. Math. Phys. **168**, 1192 (2011).

[8] R. Melzi, P. Carretta, A. Lascialfari et al., Phys. Rev. Lett. **85**, 1318 (2000).

[9] R. Melzi, S. Aldrovandi, F. Tedoldi et al., Phys. Rev. B **64**, 024409 (2001).

[10] H. Rosner, R. R. P. Singh, W. H. Zheng et al., Phys. Rev. B **67**, 014416 (2003).

[11] J. M. Tranquada, in J. R. Schrieffer and J. S. Brooks, eds., *Handbook of High-Temperature Superconductivity*, Springer New York, 257–298 (2007).

[12] E. E. Kaul, H. Rosner, N. Shannon et al., J. Magn. Magn. Mater. **272–276, Part 2**, 922 (2004).

[13] M. Skoulatos, J. Goff, N. Shannon et al., J. Magn. Magn. Mater. **310**, 1257 (2007).

[14] P. Carretta, M. Filibian, R. Nath et al., Phys. Rev. B **79**, 224432 (2009).

[15] M. Skoulatos, J. P. Goff, C. Geibel et al., Europhys. Lett. **88**, 57005 (2009).

[16] H. Kageyama, T. Kitano, N. Oba et al., J. Phys. Soc. Jpn. **74**, 1702 (2005).

[17] A. A. Tsirlin and H. Rosner, Phys. Rev. B **79**, 214417 (2009).

[18] A. A. Tsirlin, B. Schmidt, Y. Skourski et al., Phys. Rev. B **80**, 132407 (2009).

[19] R. Nath, A. A. Tsirlin, H. Rosner et al., Phys. Rev. B **78**, 064422 (2008).

[20] S. Feldkemper, W. Weber, J. Schulenburg et al., Phys. Rev. B **52**, 313 (1995).

[21] S. Feldkemper and W. Weber, Phys. Rev. B **57**, 7755 (1998).

[22] H. Manaka, T. Koide, T. Shidara et al., Phys. Rev. B **68**, 184412 (2003).

[23] D. Kasinathan, A. B. Kyker, and D. J. Singh, Phys. Rev. B **73**, 214420 (2006).

[24] J. Richter, J. Schulenburg, and A. Honecker, in U. Schollwöck, J. Richter, D. J. J. Farnell et al., eds., *Quantum Magnetism*, Springer Berlin Heidelberg, no. 645 in Lecture Notes in Physics, 85–153 (2004).

[25] N. Plakida, in *High-Temperature Cuprate Superconductors*, Springer Berlin Heidelberg, no. 166 in Springer Series in Solid-State Sciences, 377–478 (2010).

[26] Y.-Z. Ren, N.-H. Tong, and X.-C. Xie, J. Phys.: Condens. Matter **26**, 115601 (2014).

[27] M. Takahashi, Progr. Theor. Phys. Suppl. **87**, 233 (1986).

[28] M. Takahashi, Phys. Rev. Lett. **58**, 168 (1987).

[29] P. Kopietz and S. Chakravarty, Phys. Rev. B **40**, 4858 (1989).

[30] N. Karchev, Phys. Rev. B **55**, 6372 (1997).

[31] I. Juhász Junger, D. Ihle, L. Bogacz et al., Phys. Rev. B **77**, 174411 (2008).

[32] E. Manousakis and R. Salvador, Phys. Rev. B **39**, 575 (1989).

[33] Y. C. Chen, H. H. Chen, and F. Lee, Phys. Rev. B **43**, 11082 (1991).

[34] P. Henelius, A. W. Sandvik, C. Timm et al., Phys. Rev. B **61**, 364 (2000).

[35] J. Kondo and K. Yamaji, Prog. Theor. Phys. **47**, 807 (1972).

[36] H. Shimahara and S. Takada, J. Phys. Soc. Jpn. **60**, 2394 (1991).

[37] F. Suzuki, N. Shimata, and C. Ishii, J. Phys. Soc. Jpn. **63**, 1539 (1994).

[38] I. Junger, D. Ihle, J. Richter et al., Phys. Rev. B **70**, 104419 (2004).

[39] T. N. Antsygina, M. I. Poltavskaya, I. I. Poltavsky et al., Phys. Rev. B **77**, 024407 (2008).

[40] N. Shannon, B. Schmidt, K. Penc et al., Eur. Phys. J. B **38**, 599 (2004).

[41] N. Shannon, T. Momoi, and P. Sindzingre, Phys. Rev. Lett. **96**, 027213 (2006).

[42] P. Sindzingre, N. Shannon, and T. Momoi, J. Magn. Magn. Mater. **310**, 1340 (2007).

[43] B. Schmidt, N. Shannon, and P. Thalmeier, J. Phys.: Condens. Matter **19**, 145211 (2007).

[44] B. Schmidt, N. Shannon, and P. Thalmeier, J. Magn. Magn. Mater. **310**, 1231 (2007).

[45] J. R. Viana and J. R. de Sousa, Phys. Rev. B **75**, 052403 (2007).

[46] P. Sindzingre, L. Seabra, N. Shannon et al., J. Phys.: Conf. Ser. **145**, 012048 (2009).

[47] R. Shindou and T. Momoi, Phys. Rev. B **80**, 064410 (2009).

[48] M. Härtel, J. Richter, D. Ihle et al., Phys. Rev. B **81**, 174421 (2010).

[49] M. Härtel, J. Richter, O. Götze et al., Phys. Rev. B **87**, 054412 (2013).

[50] D. V. Dmitriev, V. Y. Krivnov, and A. A. Ovchinnikov, Phys. Rev. B **55**, 3620 (1997).

[51] J. Richter, A. Lohmann, H.-J. Schmidt et al., J. Phys.: Conf. Ser. **529**, 012023 (2014).

[52] M. Härtel, J. Richter, D. Ihle et al., Phys. Rev. B **78**, 174412 (2008).

[53] P. Rubin, A. Sherman, and M. Schreiber, Phys. Lett. A **376**, 1062 (2012).

[54] A. A. Vladimirov, D. Ihle, and N. M. Plakida, Eur. Phys. J. B **87**, 1 (2014).

[55] A. V. Mikheyenkov, A. V. Shvartsberg, N. A. Kozlov et al., JETP Lett. **93**, 377 (2011).

[56] A. V. Mikheyenkov, A. F. Barabanov, and A. V. Shvartsberg, Solid State Commun. **152**, 831 (2012).

[57] A. V. Mikheyenkov, A. V. Shvartsberg, and A. F. Barabanov, JETP Lett. **98**, 156 (2013).

[58] A. F. Barabanov and V. M. Berezovskii, J. Exp. Theor. Phys. **79**, 627 (1994).

[59] A. F. Barabanov and V. M. Beresovsky, J. Phys. Soc. Jpn. **63**, 3974 (1994).

[60] P. Sindzingre, N. Shannon, and T. Momoi, J. Phys.: Conf. Ser. **200**, 022058 (2010).

[61] A. W. Sandvik, in *AIP Conference Proceedings*, American Institute of Physics (2010), vol. 1297, 135–338.

[62] M. Härtel, J. Richter, D. Ihle et al., Phys. Rev. B **84**, 104411 (2011).